

$\langle 110 \rangle$ symmetric tilt grain-boundary structures in fcc metals with low stacking-fault energies

J. D. Rittner and D. N. Seidman

*Department of Materials Science and Engineering and the Materials Research Center, Northwestern University,
2225 North Campus Drive, Evanston, Illinois 60208*

(Received 4 January 1996)

Twenty-one $\langle 110 \rangle$ symmetric tilt grain boundaries (GB's) are investigated with atomistic simulations, using an embedded-atom method (EAM) potential for a low stacking-fault energy fcc metal. Lattice statics simulations with a large number of initial configurations are used to identify both the equilibrium and metastable structures at 0 K. The level of difficulty in finding the equilibrium structures is quantitatively assessed. The stability of the structures at an elevated temperature is investigated by Monte Carlo annealing. A form of GB dissociation is identified in a number of the boundaries. These structures are used to develop a dislocation model of GB dissociation by stacking-fault emission. Also, an attempt is made to apply the structural unit model (SUM) to the simulated boundaries and problems that are encountered for GB structures in low stacking-fault energy metals are enumerated and discussed. [S0163-1829(96)01734-1]

I. INTRODUCTION

The atomic structure of grain boundaries (GB's) has been the subject of intense interest for many years. A primary reason is the influence atomic structure has on many GB properties such as segregation,¹ GB diffusion,² GB mobility and sliding,³ precipitation,⁴ corrosion,⁵ intergranular fracture,⁶ etc., which in turn, may have a significant impact on the macroscopic properties of the material. The structure of GB's is a function of five macroscopic geometrical degrees of freedom (DOF), which are thermodynamic state variables,⁷ in addition to the conventional state variables temperature, pressure, and bulk composition. The five DOF can be defined as the rotation axis \hat{c} , the rotation angle θ , and the boundary plane unit normal \hat{n} . If \hat{c} is perpendicular to \hat{n} , the GB is called a tilt boundary (see Fig. 1). If, in addition, \hat{n} is the same in both grains then the GB is a symmetric tilt boundary. Although tilt GB's occupy only an infinitely small portion of the five-dimensional geometric GB phase space,⁸ they are frequently observed experimentally, which suggests that they are energetically favored over other types of GB's.⁹

In this research we focus on symmetric tilt GB's with a $\langle 110 \rangle$ tilt axis. A set of 21 different boundaries, listed in Table I, are simulated using an embedded atom method

(EAM) potential for a low stacking-fault energy (SFE) fcc metal. The computational procedure that is employed (Sec. II) allows both the equilibrium and metastable structures of each boundary at 0 K to be found. The stability of these structures at an elevated temperature is also investigated.

Results from the simulations are presented in Sec. III. First, several general results, including the GB energies, multiplicity of structures, and the stability of the structures, for all 21 boundaries are given. A new quantity called the "accessibility" of a structure is also introduced. Next, the 0 K equilibrium structures for each of the 21 boundaries are presented. Two of these boundaries have unusual structures with atomic relaxations along the tilt axis. The equilibrium structures for six boundaries simulated with a high-SFE EAM potential are also shown for comparison.

The 0 K equilibrium structures are used to discuss two main topics: GB dissociation by the emission of stacking faults (Sec. IV A) and the structural unit model (SUM) description of GB structures (Sec. IV B). Several recent studies^{10,11} of GB's in low-SFE fcc metals have detected GB structures that have a width of about 1 nm. Similar wide GB structures are found in our research and are used to develop a model of GB dissociation by stacking-fault emission. Two examples of the application of this model are presented. The SUM was developed from a detailed study¹² of the atomic structures of several $\langle 110 \rangle$ symmetric tilt GB's simulated using a pairwise potential for a fcc metal with a fairly high SFE. Although the SUM has been widely used for describing GB structures in many materials, it is not found to be useful for the low-SFE structures. Possible reasons for problems with the SUM description are discussed. Finally, the main conclusions are summarized in Sec. V.

II. PROCEDURE

A. Computational cell and border conditions

The simulations are performed using computational cells containing a bicrystal with a boundary plane at its center. The geometry and dimensions of the computational cells are

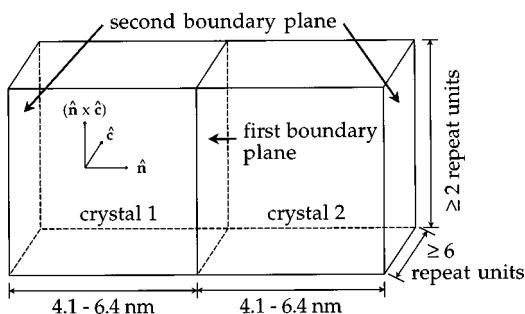


FIG. 1. Schematic of the bicrystal computational cells showing typical dimensions.

TABLE I. The geometric parameters used to identify the 21 GB's and two perfect crystal orientations. The number of initial configurations and the results from the lattice statics and Monte Carlo simulations are given for each GB.

Σ value and boundary plane	$\langle 110 \rangle$ tilt angle	Number of initial configurations	Number of structures at 0 K	Accessibility of 0 K equilibrium structure (%)	Number of stable structures at 800 K
$\Sigma = 1/(001)$	0°				
$\Sigma = 73/(1,1,12)$	13.44°	96	19	4	12
$\Sigma = 33/(118)$	20.05°	88	22	2	9
$\Sigma = 19/(116)$	26.53°	76	15	7	7
$\Sigma = 27/(115)$	31.59°	72	4	1	1
$\Sigma = 9/(114)$	38.94°	36	7	6	2
$\Sigma = 57/(227)$	44.00°	76	13	24	3
$\Sigma = 11/(113)$	50.48°	44	1	100	1
$\Sigma = 33/(225)$	58.99°	88	9	60	1
$\Sigma = 3/(112)$	70.53°	24	2	75	1
$\Sigma = 43/(335)$	80.63°	88	5	61	5
$\Sigma = 17/(223)$	86.63°	68	7	46	6
$\Sigma = 17/(334)$	93.37°	68	11	1	8
$\Sigma = 43/(556)$	99.37°	84	20	2	15
$\Sigma = 3/(111)$	109.47°	24	1	100	1
$\Sigma = 33/(554)$	121.01°	88	10	5	9
$\Sigma = 11/(332)$	129.52°	44	5	61	3
$\Sigma = 9/(221)$	141.06°	36	2	58	1
$\Sigma = 27/(552)$	148.41°	108	22	17	3
$\Sigma = 19/(331)$	153.47°	76	4	3	1
$\Sigma = 3/(441)$	159.95°	88	6	14	3
$\Sigma = 73/(661)$	166.56°	96	23	15	4
$\Sigma = 1/(110)$	180°				

shown in Fig. 1. Atomic positions in the bicrystals are generated from geometrical coincident site lattice (CSL) constructions. Three-dimensional Born–von Karman periodic border conditions¹³ are employed to eliminate surface effects. The periodic borders generate a second GB with the same misorientation and boundary plane at the sides of the computational cell in the \hat{n} direction. Since there are no fixed regions in the cell, rigid-body translations (RBT's) between the two crystals are free to occur if they are energetically favorable. The shape of the cell is not permitted to change during the simulations. It is noted that these border conditions cannot be used for all types of GB's. When periodic border conditions are used and the shape of the computational cell is not permitted to change, RBT's at the two boundaries in the cell occur in opposite directions. In some boundaries, such as asymmetric GB's, this can result in the creation of different structures at the two boundaries. For $\langle 110 \rangle$ symmetric tilt GB's, however, the structures of the two boundaries are identical.

Although periodic border conditions eliminate surface effects, the computational cells must still be large enough to prevent interactions between the two parallel boundaries and other finite-size effects. The crystals are from 4.1 to 6.4 nm wide for the cells used in this research. The atomic relaxations that occur at the boundary during a simulation may reduce the periodicity of the GB structure. To allow for such relaxations, at least six CSL periods in the \hat{c} direction along the tilt axis and two in the $(\hat{n} \times \hat{c})$ direction are used. With

these minimum dimensions, the cells contain a total of 6336 to 10 640 atoms depending on the boundary.

The periodic borders of the cell parallel to the boundary plane are permitted to move during the simulations to allow for volume expansion at the boundary. The periodic borders perpendicular to the boundary plane are kept immobile to counteract the interfacial free energy of the GB and maintain the correct equilibrium lattice constant in the bulk crystal regions. These border conditions result in a constant zero pressure in the computational cell during the simulations. This procedure has been shown¹⁴ to yield results equivalent to using mobile borders and much larger bulk crystal regions that require longer computation times.

A separate set of simulations are used to calculate the equilibrium lattice constants at both 0 and 800 K. These simulations use a computational cell containing a perfect crystal with 500 atoms. Lattice statics simulations are used to find the 0 K lattice constants and Monte Carlo simulations are used to find the lattice constants at 800 K. Unlike the GB simulations, all of the periodic borders are permitted to move so that a crystal can reach its equilibrium lattice spacing at zero pressure.

B. Interaction potentials

The atomic interactions are calculated with potentials based on the EAM formalism.¹⁵ EAM potentials have the functional form

$$E = \sum_i F_i(N_i) + \sum_i \sum_{j, j \neq i} \Phi_{ij}(R_{ij}), \quad (1)$$

where F_i is the embedding energy associated with placing an atom into the total electron density N_i due to all the atoms in the system. The term $\Phi_{ij}(R_{ij})$ is a pairwise core-core interaction function. The total electron density at a site i is given by

$$N_i = \sum_{j, j \neq i} \rho_j(R_{ij}), \quad (2)$$

where $\rho_j(R_{ij})$ is the radial electron density function of atom j at a distance R_{ij} . To model a particular element, the three functions F , Φ , and ρ are fitted to experimental values and in some cases, first-principles results.¹⁶

Since the electron density functions are assumed to be radially symmetric, EAM potentials are best suited to modeling elements whose bonding is primarily nondirectional, such as metals that crystallize in the fcc structure. Without the embedding energy term, EAM potentials are functionally equivalent to radially symmetric pair potentials. EAM potentials are more sensitive to changes in atomic coordination than pair potentials because of the embedding energy. Coordination effects can be very important when the local density deviates from the ideal value, such as at surfaces and GB's. When the coordination is reduced, bond lengths shorten, resulting in more densely packed structures than are found with pair potentials that ignore coordination effects. Despite the additional complexity of the EAM potentials they are still relatively fast to compute with, allowing for simulations with the large numbers of atoms required to study GB's. The EAM potentials have been used successfully in a wide range of applications.¹⁷

In this research, an EAM potential is used to represent an fcc metal with a low SFE. EAM potentials naturally tend to underestimate the SFE because of their functional form.¹⁸ It is possible to force EAM potentials to fit the correct SFE of a material, but this may be at the expense of other properties. Except where noted otherwise, the simulations are performed with an EAM potential for nickel.¹⁹ Although the experimental SFE of Ni is high (128 mJ m^{-2}),²⁰ the SFE for the EAM Ni potential (14 mJ m^{-2}) is closer to the experimental SFE of silver (22 mJ m^{-2}).²⁰ Thus, the simulations with this potential are interpreted as describing a generic fcc metal with a low SFE. Although only a few pure metals, such as silver, gold, and copper, have low SFE's, it has been found that alloying generally lowers the SFE in most materials.²¹ Also, low SFE's are found in many common engineering materials such as austenitic stainless steels. For comparison, a few additional simulations are performed using an EAM potential for aluminum which has a much higher SFE (104 mJ m^{-2}).²²

Simulations on $[1\bar{1}0]$ tilt boundaries in aluminum have been performed previously¹² using a pairwise potential. This so-called DRT potential for aluminum²³ contains long-range Friedel oscillations that have significant amplitudes even at large interatomic distances. Due to the Friedel oscillations, the SFE varies with the cutoff radius. For cutoffs greater than $15a_0$, where a_0 is the lattice constant, the SFE converges to about 105 mJ m^{-2} .²⁴ For faster computations a much

smaller cutoff of $1.6a_0$ was used in Ref. 12. For this cutoff radius the SFE appears to be much higher, around 200 mJ m^{-2} . Despite the differences in their SFE's and functional forms, the EAM and DRT potentials for aluminum produce very similar structures which are discussed in Sec. III B 7.

C. Lattice statics simulations

Relaxed 0 K GB structures are found with lattice statics simulations. Lattice statics is an energy minimization technique that finds the nearest local energy minimum for a given initial configuration. There are, however, no assurances that the equilibrium configuration of atoms corresponding to the global energy minimum has been reached. To improve the chances of finding the structure with the lowest GB energy, i.e., the structure that is in equilibrium at 0 K, a number of different initial configurations are used. The other structures that are found that have higher GB energies are metastable at 0 K. There are different ways to generate initial configurations, including using random MC configurations²⁵ and the procedure used here, which is based on varying the RBT of the bicrystal. The RBT vector \mathbf{t} , can be separated into a two-component in-plane translation \mathbf{p}'_i , and a volume expansion perpendicular to the boundary \mathbf{e} .²⁶ The range of unique in-plane translations is defined by the cell of nonidentical displacements (CNID's).²⁷ The CNID is divided into a grid of points so that the in-plane translation is sampled uniformly. The displacement-shift-complete (DSC) lattice is used as the basis of the grid, since the density of the DSC lattice is related to the size of the CNID for tilt boundaries.²⁸ A grid spacing of 0.25 DSC vectors or $(a_0/8)[1\bar{1}0]$ in the $\hat{\mathbf{c}}$ direction along the tilt axis is used for each boundary. The grid spacing in the $(\hat{\mathbf{n}} \times \hat{\mathbf{c}})$ direction varies from 0.5 to 3.0 DSC vectors, depending on the boundary. The origin of the grid in the plane of the boundary is shifted slightly off a coincidence lattice site to break the initial symmetry of the bicrystal. The initial value used for the RBT normal to the boundary plane \mathbf{e} is 0 nm or, to speed up the volume relaxation, 0.02 nm. These grid spacings result in a set of 24–108 initial configurations for each boundary, as shown in the third column of Table I. If a large number of structures exist for a boundary, they can only be found by using a large number of initial configurations. The lattice statics simulations employ the conjugate gradient minimization technique²⁹ and are terminated when the maximum change in the atomic positions from one step to the next is less than 10^{-7} nm.

D. Monte Carlo annealing

Lattice statics simulations generate GB structures that correspond to local energy minima at 0 K. The GB energy, or the relative depth of each minimum, is also determined. These simulations cannot, however, provide any information about the heights of the energy barriers separating the minima. The thermal fluctuations that are present at elevated temperatures may be sufficient to overcome these energy barriers and allow a structure to relax to a lower energy structure. If this is true, then the structure is not physically significant since it will be unstable at elevated temperatures. Thus, with lattice statics alone it is not possible to determine

if the structures found are physically significant at elevated temperatures. To test the stability of the 0 K GB structures against thermal fluctuations, they are annealed with Monte Carlo (MC) simulations. In this context, a stable structure is defined as one in which the atomic positions do not change after MC annealing. If the average coordinates of even a single atom have changed from the initial structure,³⁰ that structure is said to be unstable.

Monte Carlo simulations statistically sample different atomic configurations at a given temperature. Thermal fluctuations are implicitly included in these different configurations, and as a result it is possible for MC simulations to overcome the energy barrier between different structures. The length of time that a system spends in a particular structure is proportional to $\exp(-E/kT)$, where E is the internal energy and kT has its usual significance. A system will move between its various structures but only the structures with the lowest energies are found with any appreciable frequency. If the energy barriers between the structures are high enough, relative to the thermal fluctuations (kT), the time it takes to move from one low-energy structure to another approaches infinity. Thus, it is possible for a system to be trapped in a structure that is not the equilibrium structure. Monte Carlo simulations can be used to anneal a structure for a certain length of time at a given temperature to test its stability. A MC anneal of 10^4 steps per atom, with an additional 10^3 steps per atom for the initial equilibration, at a temperature of 800 K is used to test the stability of the structures in this research. It is anticipated that the number of stable structures generally decreases as the annealing time and/or temperature is increased.

III. RESULTS

A. General results

1. Grain-boundary energies

A total of 21 $\langle 110 \rangle$ symmetric tilt boundaries spanning the entire range of unique tilt angles have been investigated. Using the standard CSL notation, the boundaries and their tilt angles are listed in the first two columns of Table I. The perfect crystal orientations corresponding to the $\Sigma = 1/(001)/0^\circ$ and $\Sigma = 1/(110)/180^\circ$ ‘‘boundaries’’ are included as the end points of this tilt-angle range. The GB energy is plotted in Fig. 2 as a function of the tilt angle for the 0 K equilibrium structure of each boundary. This range of boundaries is unique in that there are two deep cusps in the GB energy for high-angle boundaries. The cusps are for the $\Sigma = 11/(113)/50.48^\circ$ and $\Sigma = 3/(111)/109.47^\circ$ coherent twin boundaries. An earlier investigation³¹ of the variation of GB energies for a wide range of boundaries found that, in general, the energies of high-angle boundaries are fairly uniform with only shallow energy cusps. In contrast to the majority of the boundaries investigated, the same two deep cusps were found in $\langle 110 \rangle$ symmetric tilt boundaries for several fcc metals. The same cusps have also been found in experimental measurements of GB energies in aluminum.³² A larger number of GB’s would be required to identify conclusively any shallower cusps in Fig. 2.

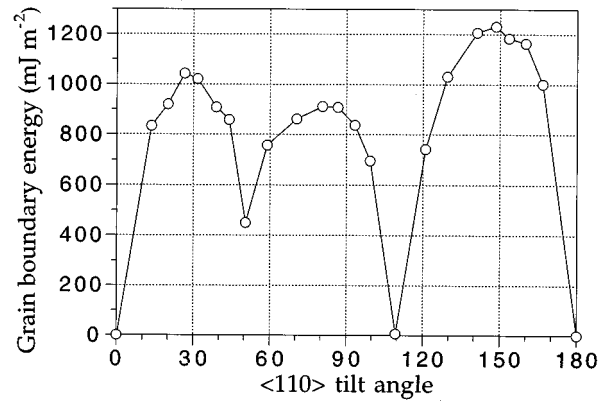


FIG. 2. Grain-boundary energies of the 0 K equilibrium structures for 21 $\langle 110 \rangle$ symmetric tilt boundaries as a function of the tilt angle. The two deep cusps are the $\Sigma = 11/(113)/50.48^\circ$ and $\Sigma = 3/(111)/109.47^\circ$ coherent twin boundaries.

2. Multiplicity of structures and accessibility

A large number of relaxed structures are found for most of the boundaries as shown in the fourth column of Table I. It is important to note that these structures are not symmetry related²⁶ but are unique structures with different GB energies. The range of GB energies covered by the different structures of a particular boundary can be small, especially when there are only a few structures, but it is often quite large. The range of GB energies for three boundaries are shown along the horizontal axes in Fig. 3. The highest GB energy for the $\Sigma = 27/(115)/31.59^\circ$ boundary [Fig. 3(a)] is only 40 mJ m^{-2} higher than the lowest energy. Much wider ranges of 140 and 270 mJ m^{-2} are found for the $\Sigma = 19/(116)/26.53^\circ$ [Fig. 3(b)] and $\Sigma = 17/(223)/86.63^\circ$ [Fig. 3(c)] boundaries, respectively. The different structures of these boundaries are far from being energetically degenerate.

The number of structures found is roughly proportional to the area of the CNID for each boundary. As the size of the CNID decreases the variation of the GB energy with changes in the RBT must also decrease.³³ Thus, it is expected that boundaries with smaller CNID’s will have fewer structures. This may explain why the multiplicity of structures found for tilt boundaries is usually larger than it is for twist boundaries which typically have much smaller CNID’s.

Although it may be possible to find a large number of structures when using a minimization technique such as lattice statics, it is generally expected that the majority of the initial configurations will relax to the equilibrium structure. Thus, it is often assumed that only a small number of initial configurations are required to find the equilibrium structure of a boundary and that using a larger number of initial configurations will only result in more metastable structures being found. To investigate the validity of this assumption, the accessibilities of the 0 K equilibrium structures are examined. We define the accessibility of a final structure as the percentage of the set of initial configurations that relax to that structure. The accessibilities of the structures for the three boundaries in Fig. 3 are plotted along the vertical axes. For some boundaries, such as the $\Sigma = 17/(223)/86.63^\circ$ GB [Fig. 3(c)], the equilibrium structure is the most accessible.

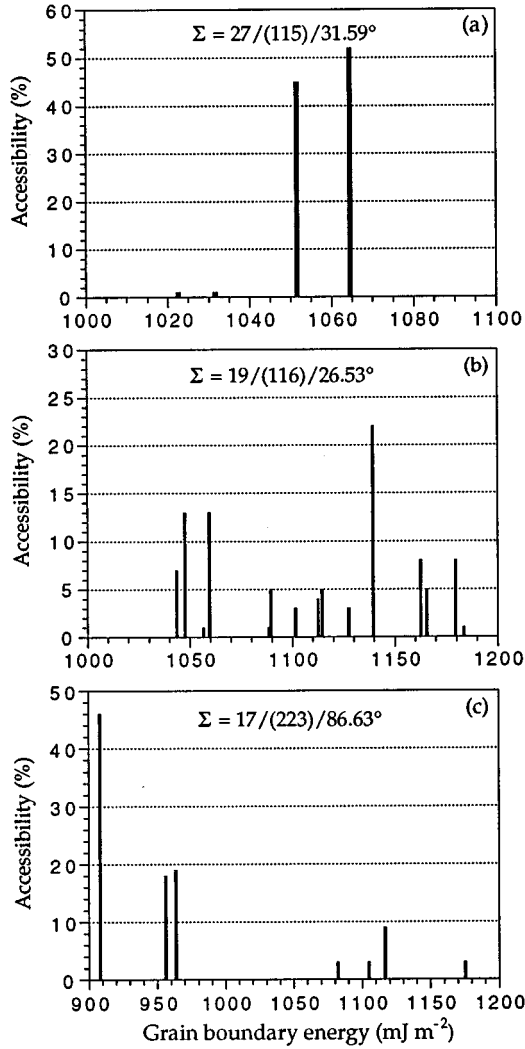


FIG. 3. Accessibility vs GB energy for multiple structures of three typical boundaries: (a) $\Sigma = 27/(115)/31.59^\circ$, (b) $\Sigma = 19/(116)/26.53^\circ$, and (c) $\Sigma = 17/(223)/86.63^\circ$.

For the majority of the boundaries, however, the accessibility of the equilibrium structure is 15% or less. The accessibility of the 0 K equilibrium structure for each boundary is shown in the penultimate column of Table I. One extreme case is the $\Sigma = 27/(115)/31.59^\circ$ boundary [Fig. 3(a)], where only one out of the set of 72 initial configurations relaxed to the equilibrium structure. If a smaller set of initial configurations had been used, it is very unlikely that this structure would have been found. It is possible that structures with even lower energies may be found if a larger set of initial configurations are used. If such structures are found, they must have very small accessibilities. It should be noted that the accessibility is strictly defined only for a given set of initial configurations and may change slightly if a different set is used. The accessibility of structures is a very important consideration when using an energy minimization technique such as lattice statics.

3. Stability of structures at an elevated temperature

The stability of the structures against thermal fluctuations at an elevated temperature is investigated by annealing them

with Monte Carlo simulations. With only one exception, the 0 K equilibrium structure for each boundary remained stable during the annealing. The exception is the 0 K equilibrium structure of the $\Sigma = 57/(227)/44.00^\circ$ boundary which relaxed to the metastable structure with the second lowest-energy at 0 K. This is an indication of a possible GB phase change that occurs at elevated temperatures. The stability of the 0 K equilibrium structures found is not a guarantee that other structures with even lower energies do not exist. Many of the 0 K metastable structures that are unstable at higher temperatures, however, relaxed to the 0 K equilibrium structures, so it appears likely that they are in fact the equilibrium structures for these boundaries. In the $\Sigma = 27/(115)/31.59^\circ$ boundary [Fig. 3(a)], for example, all three of the 0 K metastable structures relaxed to the equilibrium structure.

In most boundaries, however, some of the 0 K metastable structures remain stable during the annealing. For example, six of the seven structures for the $\Sigma = 17/(223)/86.63^\circ$ boundary [Fig. 3(c)] remained stable. The number of structures that remained stable for each boundary is given in the last column of Table I. Over half of the boundaries had three or more stable structures and one, the $\Sigma = 43/(556)/99.37^\circ$ boundary, had as many as 15 stable structures. Even at a temperature of 800 K, the thermal fluctuations were not large enough to overcome many of the energy barriers separating the different GB structures. Thus, GB's in real materials and those simulated with elevated temperature techniques such as MC, can be trapped in metastable structures. With anneals of different times or at different temperatures, the number of structures that are stable against thermal fluctuations will most likely change.

B. Equilibrium structures

1. Identification of grain boundary structures

To simplify comparison of GB structures, a standard procedure is used so that they may be uniquely characterized. After a computational cell has been relaxed with lattice statics or Monte Carlo simulations, the atoms are partitioned into GB and bulk-crystal regions. The bulk-crystal regions contain all atoms that are part of a contiguous array of tetrahedra. The tetrahedron is the smallest of five random close-packed structural units (SU's) that were discovered³⁴ in close-packed liquids. It is also the smallest SU that completely tiles the perfect crystal in a $\langle 110 \rangle$ projection. It is formed by two nearest-neighbor atoms in one $(\bar{2}\bar{2}0)$ plane and an additional nearest neighbor in the $(\bar{2}\bar{2}0)$ planes both above and below the first. The A SU, three of which are shown in Fig. 4(a) for the $\Sigma = 1/(001)/0^\circ$ perfect crystal orientation, is comprised of two tetrahedral units with two atoms in common on the middle $(\bar{2}\bar{2}0)$ plane. To differentiate the GB region from the bulk-crystal regions, a line is drawn wherever the atoms cannot be grouped into tetrahedral units. A line is also drawn if there is a sharp change in the orientation of the tetrahedral units, such that the tiling pattern is disrupted. The change from the bulk crystal to the GB region is often not very sharp. Following the limit used in Ref. 34, distortions of up to 15% in a tetrahedral unit's nearest-neighbor distances are allowed in the bulk-crystal regions. Atoms in the GB region are further divided into SU's that are consistent with the SU's of other nearby boundaries, if pos-

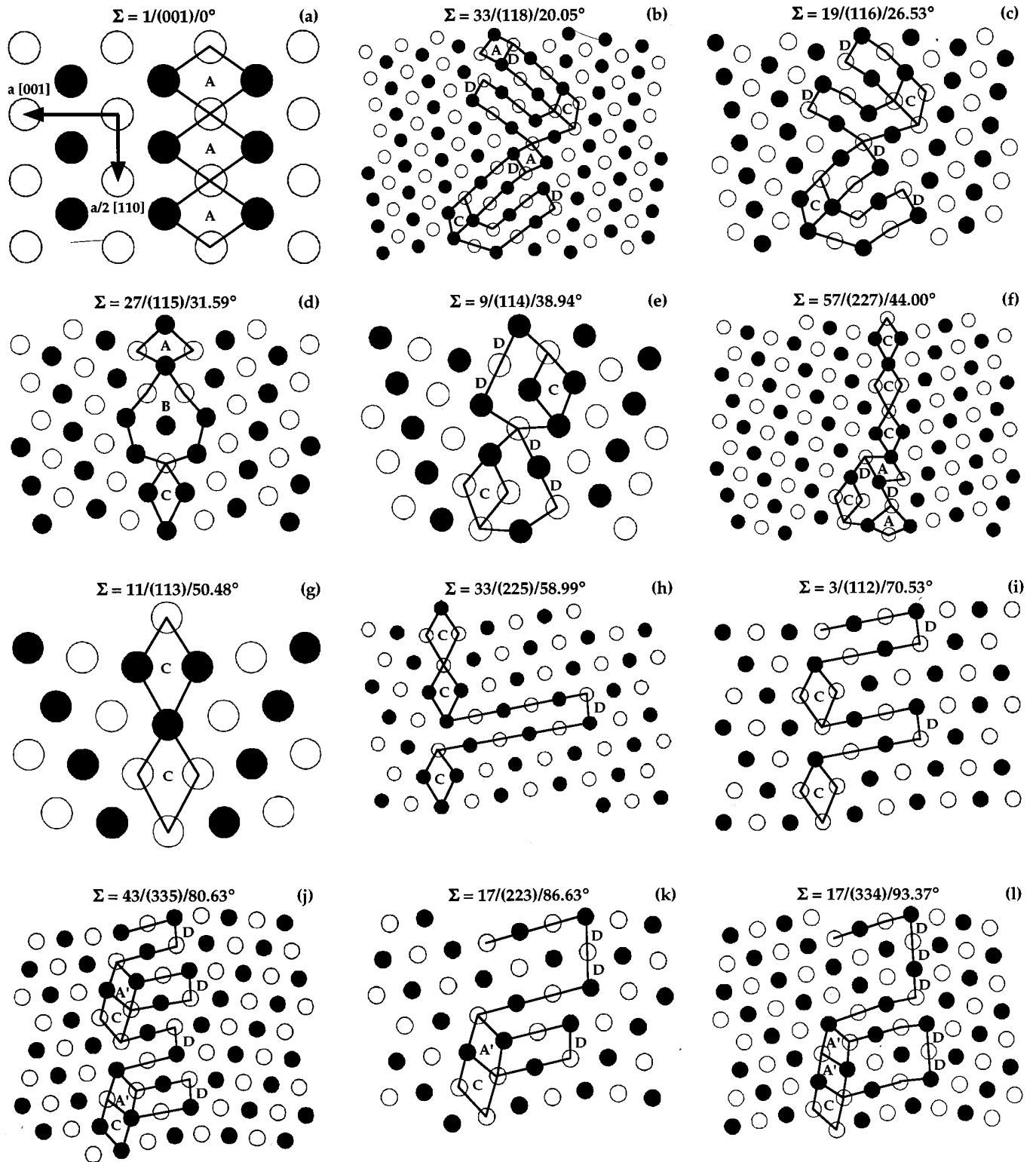


FIG. 4. Equilibrium structures of 19 $\langle 110 \rangle$ symmetric tilt boundaries and two perfect crystal orientations simulated with an EAM potential that has a low stacking-fault energy. The GB region is outlined and separated into structural units as discussed in Sec. III B 1.

sible. To reduce the number of distinct SU's, distortions exceeding 15% are occasionally permitted in the SU's of the GB region. The flexibility with which SU's can be defined has been explored previously.³⁵

The 0 K equilibrium structures for each of the 21 boundaries are characterized using this procedure. The boundaries are divided into four tilt-angle ranges based on similarities

between their structures. The $\Sigma = 73/(1,1,12)/13.44^\circ$ and $\Sigma = 43/(556)/99.37^\circ$ boundaries are discussed in a separate section (Sec. III B 6) on structures that have relaxations along the $[1\bar{1}0]$ tilt axis. Finally, six additional structures simulated with a high-SFE potential are presented for comparison in Sec. III B 7.

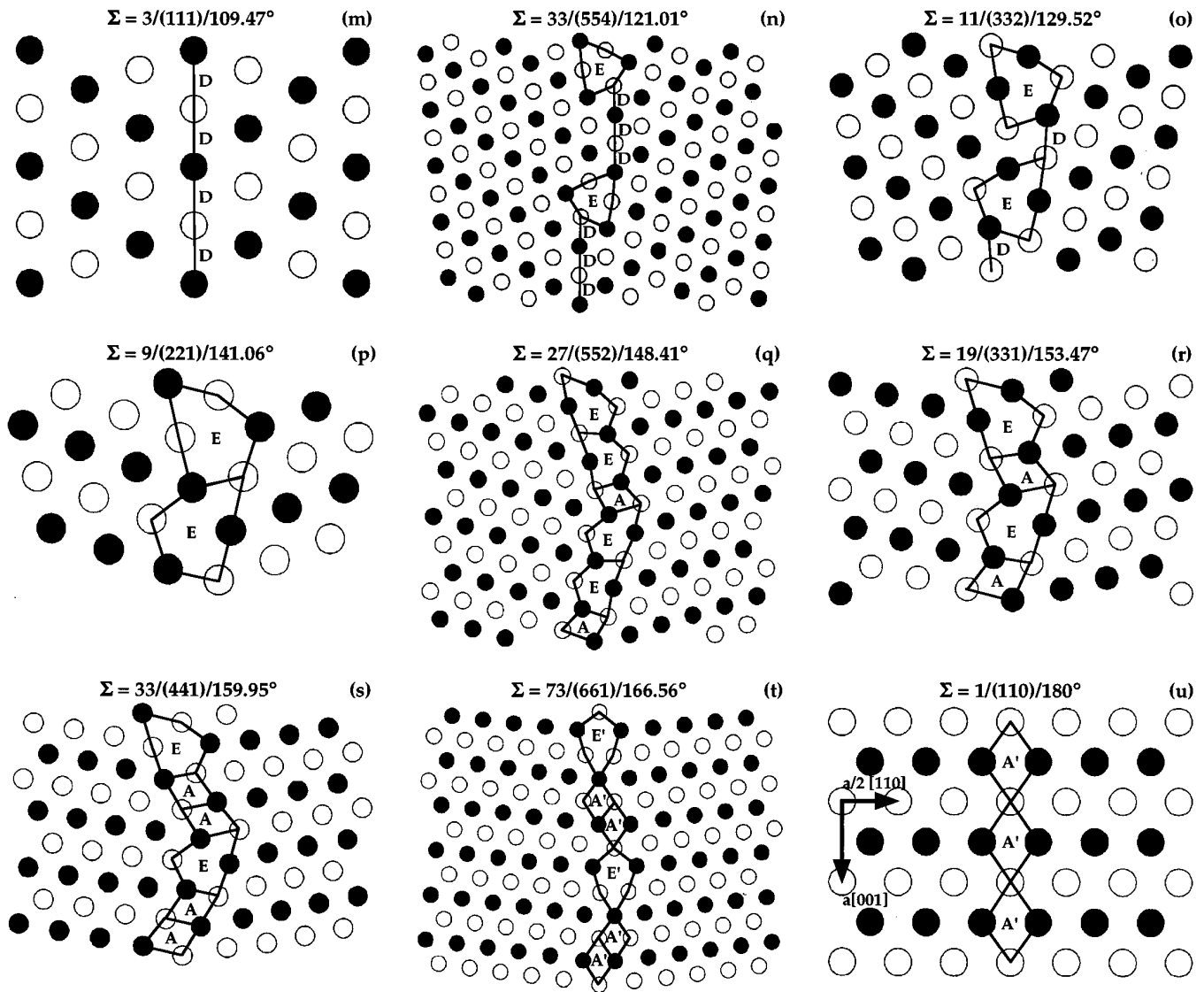


FIG. 4. (Continued).

2. Tilt angle range 1: $\theta=0^\circ-50.48^\circ$

The 0 K equilibrium structures for seven boundaries with tilt angles between $\theta=0^\circ$ and 50.48° are shown in Figs. 4(a)–4(g). The structures are viewed along the $[1\bar{1}0]$ tilt axis and the atoms in two consecutive $(2\bar{2}0)$ planes perpendicular to this axis are shown as black or white. There are three primary SU's found in these boundaries: (1) the A SU from the $\Sigma=1/(001)/0^\circ$ perfect crystal orientation [Fig. 4(a)]; (2) the C SU from the $\Sigma=11/(113)/50.48^\circ$ boundary [Fig. 4(g)]; and (3) the D SU from $\Sigma=3/(111)/109.47^\circ$ boundary [Fig. 4(m)]. As is discussed in more detail in the next section, the D SU is closely related to a Shockley partial dislocation and is frequently found terminating a ribbon of intrinsic stacking fault. This is seen in the $\Sigma=33/(118)/20.05^\circ$ [Fig. 4(b)] and $\Sigma=19/(116)/26.53^\circ$ [Fig. 4(c)] boundaries where two stacking faults extend from each C SU. The presence of stacking faults indicates that the GB dislocation cores are not localized in these boundaries. In the $\Sigma=9/(114)/38.94^\circ$ [Fig. 4(e)] and $\Sigma=57/(227)/44.00^\circ$ [Fig. 4(f)] boundaries there are also two D SU's associated

with C SU's but since they are next to each other and closer to the C SU, separate stacking faults are not observed. In the $\Sigma=57/(227)/44.00^\circ$ boundary there are three plain C SU's and a fourth with D SU's that is shifted to one side by GB steps consisting of distorted A SU's.

The $\Sigma=27/(115)/31.59^\circ$ boundary [Fig. 4(d)] is unique in that it does not contain any D SU's or stacking faults, and the B SU that is found in this boundary is not found in any other boundary. The B SU is labeled as a primary SU to simplify comparison with boundary structures that are found in higher-SFE metals that are discussed in Sec. III B 7. This is a so-called centered boundary¹² because its CSL is base-centered orthorhombic and the base-centered plane is parallel to the boundary plane. Centered boundaries have two CSL sites in each boundary period with one site displaced by $(a_0/4)[1\bar{1}0]$ along the tilt axis with respect to the other. The structure of this boundary should have two half-periods that are identical, except for the $(a_0/4)[1\bar{1}0]$ displacement, in each boundary period. The period of the structure in Fig. 4(d), however, is equal to the full boundary period. The sym-

metry of the centered CSL is destroyed at the boundary by local atomic relaxations.

3. Tilt angle range 2: $\theta=50.48^\circ-109.47^\circ$

The 0 K equilibrium structures for seven boundaries with tilt angles between $\theta=50.48^\circ$ and 109.47° are shown in Figs. 4(g)–4(m). Three primary structural SU's are found in these boundaries; the **C** SU from the $\Sigma=11/(113)/50.48^\circ$ boundary [Fig. 4(g)], the **D** SU from the $\Sigma=3/(111)/109.47^\circ$ boundary [Fig. 4(m)], and the **A'** SU from the $\Sigma=1/(110)/180^\circ$ perfect crystal orientation [Fig. 4(u)], which is identical to the **A** SU but rotated by 90° . In all of the boundaries except for the $\Sigma=3/(111)/109.47^\circ$ boundary, **D** SU's are found terminating stacking faults that extend from the boundary planes. The structure of the **D** SU is nearly identical to the structure of a Shockley partial dislocation³⁶ that terminates an isolated intrinsic stacking fault; the only difference being a bending of the $\{111\}$ planes at the **D** SU. In the $\Sigma=3/(111)/109.47^\circ$ boundary, the $\{111\}$ planes are bent downwards by 39° at the ideal **D** SU's as they cross the boundary, whereas there is no bending of the $\{111\}$ planes at an isolated Shockley partial. The **D** SU's in the other boundaries in this tilt angle range are somewhat distorted and the bending of the $\{111\}$ planes is between 0° and -39° . In the $\Sigma=17/(223)/86.63^\circ$ [Fig. 4(k)] and $\Sigma=17/(334)/93.37^\circ$ [Fig. 4(l)] boundaries, where there are two or more adjacent **D** SU's, separate stacking faults are not formed.

The stacking faults originate from boundary planes formed by **C** and, in some cases, **A'** SU's. The **C** SU's are spaced as widely as possible by the stacking faults and their associated **D** SU's. As the tilt angle increases, the ratio of **D** SU's to **C** SU's increases. When the ratio is greater than one, **A'** SU's are also found. Each **A'** SU shifts a **D** SU and stacking fault down by one $\{111\}$ plane. The **A'** SU's keep the **D** SU's and stacking faults as widely spaced as possible. As a result of the stacking faults emanating from the boundary planes, the boundaries in this range do not have the narrow structures that are typically observed in high-angle boundaries. A more detailed analysis of these structures is given in Sec. IV A.

4. Tilt angle range 3: $\theta=109.47^\circ-141.06^\circ$

The 0 K equilibrium structures for four boundaries with tilt angles between $\theta=109.47^\circ$ and 141.06° are shown in Figs. 4(m)–4(p). There are two primary structural SU's found in these boundaries; (1) the **D** SU from the $\Sigma=3/(111)/109.47^\circ$ boundary [Fig. 4(m)], and (2) the **E** SU from the $\Sigma=9/(221)/141.06^\circ$ boundary [Fig. 4(p)]. The **E** SU could also be viewed as an elongated and rotated **C** SU. The **E** SU comes in left- and right-hand versions that are mirror images of each other. In the $\Sigma=9/(221)/141.06^\circ$ boundary the two **E** SU's are also translated by $(a_0/4)[1\bar{1}0]$ with respect to each other. The $\Sigma=33/(554)/121.01^\circ$ [Fig. 4(n)] and $\Sigma=11/(332)/129.52^\circ$ [Fig. 4(o)] boundary structures are composed of right and left-handed **E** SU's spaced as widely as possible by **D** SU's.

5. Tilt angle range 4: $\theta=141.06^\circ-180^\circ$

The 0 K equilibrium structures for six boundaries with tilt angles between $\theta=141.06^\circ$ and 180° are shown in Figs. 4(p)–4(u). There are four primary structural SU's found in these boundaries: (1) the **A** SU from the $\Sigma=1/(001)/0^\circ$ perfect crystal orientation [Fig. 4(a)]; (2) the **A'** SU from the $\Sigma=1/(110)/180^\circ$ perfect crystal orientation [Fig. 4(u)]; (3) the **E** SU from the $\Sigma=9/(221)/141.06^\circ$ boundary [Fig. 4(p)]; and the **E'** SU that is found only in the $\Sigma=73/(661)/166.56^\circ$ boundary [Fig. 4(t)]. In the $\Sigma=27/(552)/148.41^\circ$ boundary [Fig. 4(c)] there are groups of two right-handed **E** SU's and two left-handed **E** SU's separated by **A** SU's. The second **E** SU in each group is highly distorted. The **A** SU's are also tilted (one to the left and one to the right). The $\Sigma=19/(331)/153.47^\circ$ [Fig. 4(t)] and $\Sigma=33/(441)/159.95^\circ$ [Fig. 4(s)] boundary structures are similar with just a different ratio of **E** to **A** SU's. These structures are perhaps best viewed in terms of microfaceting along two asymmetric boundary plane orientations. One facet has the plane orientation $(110)_1\parallel(111)_2$, while the other has $(11\bar{1})_1\parallel(110)_2$; the subscripts indicate the facet plane in grain 1 and grain 2. Microfaceting to asymmetric orientations, where one or both interfaces are on a low-index plane, has also been observed experimentally.¹¹ The $\Sigma=73/(661)/166.56^\circ$ boundary does not fit the same pattern as the other boundaries in this range. The **E** SU's are no longer at an angle to one side or the other, but are rotated by $>90^\circ$ so that they point straight up and down. In this new orientation they are labeled **E'** SU's. Also, the **A** SU's have been replaced by the **A'** SU's from the $\Sigma=1/(110)/180^\circ$ perfect crystal orientation.

6. Structures with relaxations along the tilt axis

The 0 K equilibrium structures of the $\Sigma=73/(1,1,12)/13.44^\circ$ and $\Sigma=43/(556)/99.37^\circ$ boundaries are unusual in that there are significant relaxations along the direction of the tilt axis that disrupt the continuity of the $(2\bar{2}0)$ planes perpendicular to this direction. To visualize these structures, projections along two orthogonal directions in the plane of the boundary are shown. The projections in Figs. 5(a) and 5(c) are along the tilt axis \hat{c} , while the projections in Figs. 5(b) and 5(d) are along the $(\hat{n}\times\hat{c})$ direction (see Fig. 1). The $(2\bar{2}0)$ planes are viewed edge-on in the $(\hat{n}\times\hat{c})$ projection and the \hat{c} axis points towards the top of the page. It has been argued³⁷ on symmetry grounds that only relaxations along the tilt axis that result in continuous planes across the boundary should produce stable structures. For the $[1\bar{1}0]$ tilt boundaries this implies that the only RBT vectors permitted must have a component along the tilt axis with a magnitude of

$$\mathbf{p}_i \cdot \frac{1}{\sqrt{2}}[1\bar{1}0] = n \left(\frac{a_0\sqrt{2}}{4} \right), \quad n=0,1. \quad (3)$$

As shown in Figs. 5(b) and 5(d), the translation along the tilt axis for the $\Sigma=73/(1,1,12)/13.44^\circ$ and $\Sigma=43/(556)/99.37^\circ$ boundaries has a magnitude of $0.37(a_0\sqrt{2}/4)$ and $0.44(a_0\sqrt{2}/4)$, respectively. Thus, it appears that it is possible to have stable structures with relaxations along the tilt

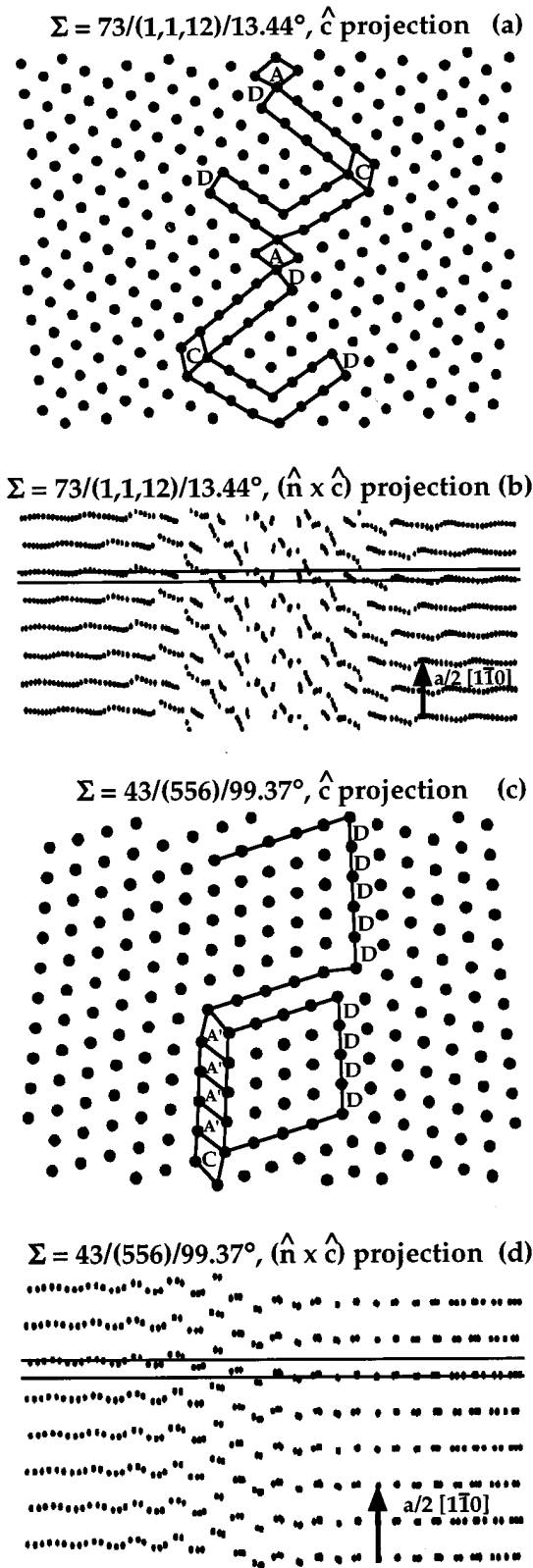


FIG. 5. Equilibrium structures of two boundaries, $\Sigma = 73/(1,1,12)/13.44^\circ$ and $\Sigma = 43/(556)/99.37^\circ$, with local atomic relaxations along the tilt axis that disrupts the $(2\bar{2}0)$ planes. The structures are viewed in projections along two orthogonal directions in the plane of the boundary. The structures are outlined in (a) and (c) as they would be if there were no relaxations along the tilt axis. The horizontal lines in (b) and (d) show the component of the rigid-body translation along the tilt axis.

axis that disrupt the continuity of the $(2\bar{2}0)$ planes across the boundary. Even though only two out of the 21 boundaries investigated have 0 K equilibrium structures of this type, they are also found in 0 K metastable structures of several boundaries. Many of these metastable structures remained stable during the MC annealing which indicates that they are not simply artifacts of the lattice statics simulations.

In Figs. 5(a) and 5(c), SU's are drawn and labeled as they would be if there were no relaxations along the tilt axis. These structures are consistent with the structures of nearby boundaries; compare Figs. 5(a) to 4(b), and Figs. 5(c) to 4(l). Occasionally a structure that has relaxations along the tilt axis is found to have the same \hat{c} projection as another structure for the same boundary in which the $(2\bar{2}0)$ planes are continuous. In such situations the arrangement of the GB dislocations in the boundary is identical and only the dislocation core structures are different. In several of these cases, the structure with the relaxations along the tilt axis has the lower GB energy. This is another indication that these are real GB structures and not artifacts of the lattice statics simulations.

The $(\hat{n} \times \hat{c})$ projections show that the relaxations along the tilt axis are different for each structure of this type. There are, however, some groups of structures that appear to have similar relaxations along the tilt axis. The structures in Fig. 5 are typical of two such groups. Segments of the $(2\bar{2}0)$ planes at the boundary in Fig. 5(b) appear to be rotated approximately 45° clockwise about the $(\hat{n} \times \hat{c})$ axis. When viewed at a glancing angle from one side, the $(2\bar{2}0)$ planes in Fig. 5(d) appear to split in two as they enter the boundary region. They combine with planes that have split from the opposite side to exit the boundary region as $(2\bar{2}0)$ planes again. Further analysis of these complicated three-dimensional structures is needed.

No experimental observations of structures of this type have been reported. This is not surprising in view of the nature of high-resolution electron microscopy (HREM) experiments. In standard HREM experiments, only a two-dimensional projection of the GB structure along the tilt axis is observed. Three-dimensional information can only be inferred from comparisons with simulated GB structures. Stereo-HREM, where the GB structure is imaged along two or more different axes in the boundary plane, is necessary to observe these structures experimentally. Other than viewing along the tilt axis, it is very difficult to find a specimen orientation where the GB is edge-on and both crystals are being viewed along a low-index direction. Currently available instruments do not have the point-to-point resolutions required to image the closely spaced atomic columns in higher-index planes.³⁸

7. High stacking-fault energy structures

For comparison with the GB structures that are found with the low-SFE potential, the boundaries in the first-tilt-angle range are simulated again using an EAM potential for aluminum²² with a high SFE. The 0 K equilibrium structures of the six boundaries in this range are shown in Figs. 6(a)–6(f). There are three primary SU's found in these boundaries: (1) the **A** SU from the $\Sigma = 1/(001)/0^\circ$ perfect crystal orientation [Fig. 4(a)]; (2) the **B** SU from the

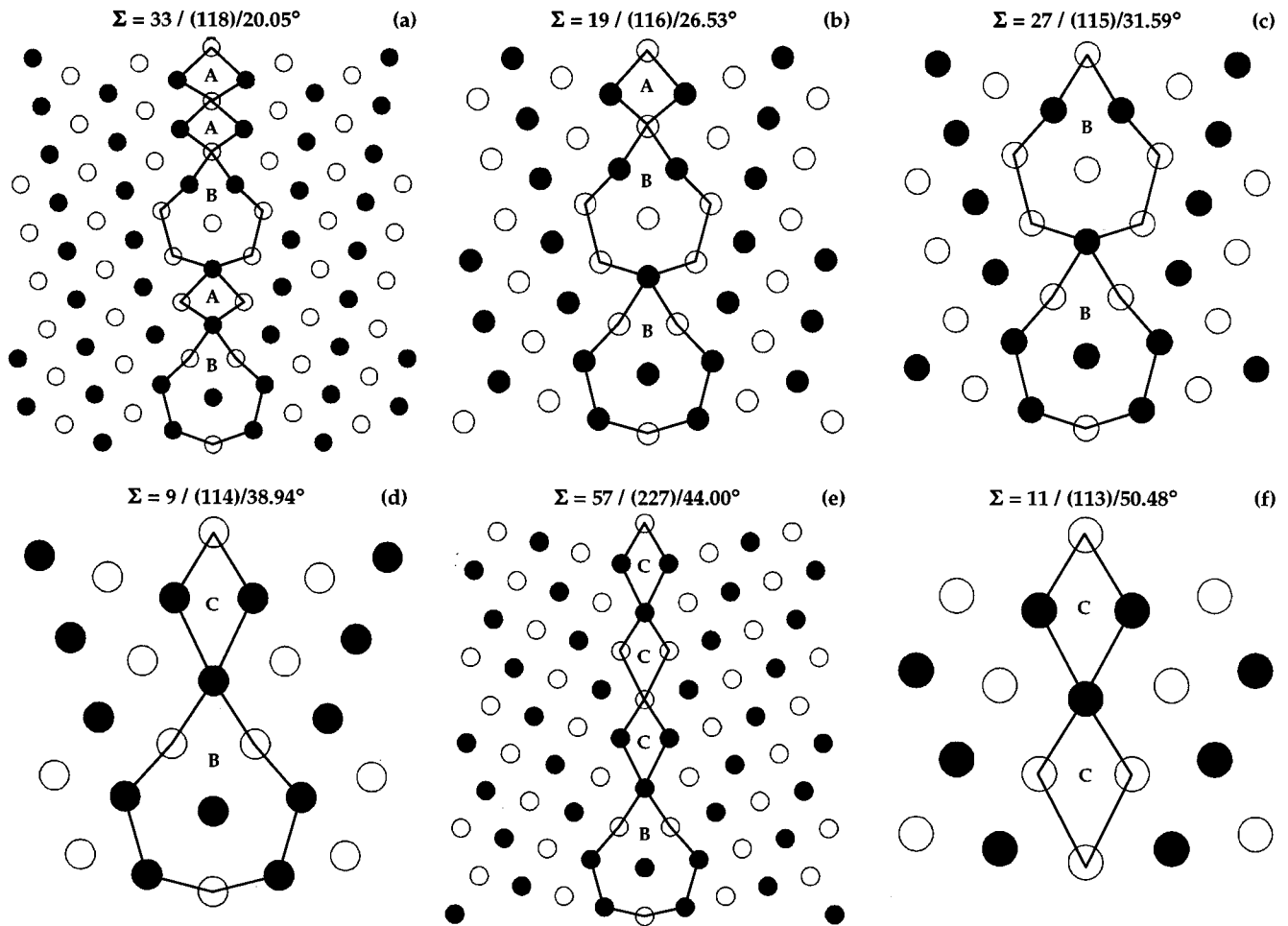


FIG. 6. Equilibrium structures of six $\langle 110 \rangle$ symmetric tilt boundaries simulated with an EAM potential that has a high stacking-fault energy. The GB region is outlined and separated into structural units as discussed in Sec. III B 1.

$\Sigma = 27 / (115) / 31.59^\circ$ boundary [Fig. 6(c)]; and (3) the C SU in the $\Sigma = 11 / (113) / 50.48^\circ$ boundary [Fig. 6(f)]. These SU's are identical to the SU's labeled with the same letters in Fig. 4. The $\Sigma = 33 / (118) / 20.05^\circ$ [Fig. 6(a)] and $\Sigma = 19 / (116) / 26.53^\circ$ [Fig. 6(b)] boundaries are composed of A and B SU's. The $\Sigma = 9 / (114) / 38.94^\circ$ [Fig. 6(d)] and $\Sigma = 57 / (227) / 44.00^\circ$ [Fig. 6(e)] boundaries are composed of B and C SU's. The GB dislocation cores are localized in these boundaries and no stacking faults are present.

IV. DISCUSSION

A. Grain-boundary dissociation by the emission of stacking faults

1. Energetics and observations of grain-boundary dissociation

The forms of GB dissociation that have been recognized previously³⁹ have one thing in common; the grain between the newly formed boundaries is free of residual defects from the dissociation process. The GB's in range 2 of Fig. 4 that have tilt angles between 50.48° and 109.47° are examples of a newly identified type of GB dissociation.⁴⁰ These boundaries have dissociated by emitting stacking faults that terminate in a wall of partial dislocations forming a second bound-

ary plane. The new grain that is formed contains many stacking faults as a result of the dissociation process. Since there is an excess energy associated with the stacking faults in the new grain, this form of GB dissociation is only energetically favorable if the following inequality is true:

$$\gamma_{1/2} > [\gamma_{1/3} + \gamma_{3/2} + F^{XS}L + \tau(L)]. \quad (4)$$

The interfacial free energy associated with the original boundary between grains 1 and 2 is $\gamma_{1/2}$. The interfacial free energies of the two new boundaries between grains 1 and 3 and 3 and 2 are given by $\gamma_{1/3}$ and $\gamma_{3/2}$, if they are isolated from each other. The excess free energy per unit volume of the new grain due to the stacking faults, with respect to a defect-free crystal, is F^{XS} . The energy associated with the interaction between the stress fields of the two new boundaries, separated by a distance L , is given by the function $\tau(L)$. To first order, $\tau(L)$ can be assumed to be positive and to decay exponentially with L .¹⁰ Since F^{XS} is positive, because of the SFE, the width of the dissociation L must be finite. With this finite dissociation, wide or so-called three-dimensional GB structures are formed. The term three-dimensional has been used to distinguish these structures from the more typical narrow or two-dimensional high-angle

TABLE II. Simulations and experimental observations of $\langle 110 \rangle$ tilt GB's with tilt angles between 50.48° and 109.47° in fcc metals.

Stacking-fault energy (mJ m^{-2})	Element	Experiment or simulation potential	GB dissociation observed?
4.7 ^a	Au	EAM potential ^b	Yes ^a
10 ^c	Cu	EAM potential ^c	Yes ^c
14 ^a	Ni	EAM potential ^c	Yes ^a
22 ^d	Ag	Experiment	Yes ^e
23 ^f	Ag	<i>N</i> -body potential ^f	Yes ^e
36 ^g	Cu	<i>N</i> -body potential ^h	Yes ^g
41 ⁱ	Cu	Pair potential ⁱ	Yes ^j
45 ^d	Au	Experiment	Yes ^{a,k,l}
78 ^d	Cu	Experiment	Yes ^m
104 ⁿ	Al	EAM potential ⁿ	No ^a
166 ^d	Al	Experiment	No ^o
≈ 200 ^p	Al	Pair potential ^q	No ^r

^aReference 40.

^bReference 19.

^cReference 48.

^dReference 20.

^eReference 44.

^fReference 53.

^gD. Hofmann and M. W. Finnis, *Acta Metall. Mater.* **42**, 3555 (1994).

^hA. J. E. Foreman, C. A. English, and W. J. Phythian, *Philos. Mag. A* **66**, 655 (1992).

ⁱA. G. Crocker, M. Doneghan, and K. W. Ingle, *Philos. Mag. A* **41**, 21 (1980).

^jReference 41.

^kReference 42.

^lReferences 11 and 43.

^mReference 45.

ⁿReference 22.

^oD. L. Medlin *et al.*, in *Atomic-Scale Imaging of Surfaces and Interfaces*, edited by D. K. Biegelson *et al.*, MRS Symposia in Proceedings No. 295 (Materials Research Society, Pittsburgh, 1993), p. 91.

^pReference 24.

^qReference 23.

^rR. C. Pond and V. Vitek, *Proc. R. Soc. London, Ser. A* **357**, 453 (1977).

GB structures. These wide structures generally do not have relaxations along the tilt axis and should not be confused with the structures discussed in Sec. III B 6. The $\Sigma = 43/(556)/99.37^\circ$ GB structure in Figs. 5(c) and 5(d), however, falls into both categories.

Many examples of these wide GB structures have recently been observed. Table II summarizes a number of simulations and experiments that have been performed on $\langle 110 \rangle$ tilt grain boundaries with tilt angles between 50.48° and 109.47° in five fcc metals. The SFE for the metal used in each experiment and for the potential employed in each simulation is given in the first column. The last column indicates if dissociated GB structures were found. For SFE's below about 80 mJ m^{-2} , GB dissociation was observed in all cases regard-

less of the metal or potential utilized. This is an indication that this mode of GB relaxation may be fairly common in low-SFE fcc metals.

Although there have been many observations of these dissociated GB structures, there has not been a completely adequate model to explain this mode of GB dissociation. In the earliest observations, the presence of stacking faults in these structures was not recognized. In a paper on Cu boundaries,⁴¹ the structures were described in terms of plane coalescence. Rigid-body translations were used to describe a boundary of this type observed in Au.⁴² Another study of GB's in Au was the first to describe the boundaries as having emitted stacking faults.⁴³ In a detailed study of the $\Sigma = 3/(112)/70.53^\circ$ boundary in Ag (Ref. 44) and Cu,⁴⁵ the presence of stacking faults was recognized but the structures were described as containing a new GB phase—the *9R* phase. This fcc polytype has a stacking fault on every third $\{111\}$ plane, such that a total of nine $\{111\}$ planes are required before the stacking sequence repeats. This is the structure found in the new grain in Fig. 4(i) between the two boundary planes. The polytype description can in principle be generalized to other boundaries but, since the spacing of the stacking faults is a function of the tilt angle, a different polytype is required to describe each boundary. For this reason, the polytype description is not useful as a general model of this form of GB dissociation. A new model has been presented,⁴⁰ and is discussed in more detail below, that is based on the language of GB dislocation theory.

2. Dissociated secondary grain-boundary dislocation model

The dissociated GB structures shown in Figs. 4(h)–4(l) can be understood by first treating the boundaries as being vicinal to either the $\Sigma = 11/(113)/50.48^\circ$ [Fig. 4(g)] or $\Sigma = 3/(111)/109.47^\circ$ [Fig. 4(m)] boundaries. As Fig. 2 demonstrates, these two coherent twin boundaries have much lower GB energies than their neighboring boundaries and are thus singular boundaries. Vicinal boundaries are GB's that are in the vicinity of such singular boundaries.⁴⁶ Any misorientation deviation between vicinal and singular GB's is accommodated by an array of secondary grain-boundary dislocations (SGBD's) in the structure of the singular boundary. A deviation in the boundary plane orientation is accommodated by steps or microfacets in the plane of the singular boundary. In this way, vicinal GB's can maintain the low-energy structure of the singular GB except for steps or microfacets and SGBD's. This is the model of vicinal high-angle boundaries from GB dislocation theory. This theory is also the basis of the structural unit model (SUM) of GB structures that is discussed in Sec. IV B.

The structures in Figs. 4(h)–4(l) are unique because the microfacets are SU's from a second singular boundary and the distortion of the SU's is reduced by dissociation of the SGBD's. Partial dislocations are emitted from the boundary forming planar defects in the perfect crystal. The partial dislocations are Shockley partials, so that relatively low-energy intrinsic stacking faults are formed. The Shockley partials are stacked in an array to one side of the original boundary creating a second boundary. Two examples are given in the following sections to illustrate this GB dissociation mechanism in more detail.

3. Example 1: vicinal $\Sigma=11/(113)/50.48^\circ$ boundary

The $\Sigma=33/(225)/58.99^\circ$ boundary [Fig. 4(h)] is vicinal to the $\Sigma=11/(113)/50.48^\circ$ [Fig. 4(g)] singular boundary. The 8.51° change in the tilt angle $\Delta\theta$ between the two boundaries is accommodated by SGBD's. The modified Read-Shockley-Frank formula⁴⁷ for symmetric tilt GB's is

$$|\mathbf{b}_{\text{SGBD}}| = 2d \sin\left(\frac{\Delta\theta}{2}\right), \quad (5)$$

where d is the repeat period of the boundary and \mathbf{b}_{SGBD} is the total Burgers vector of the SGBD's required to produce the change $\Delta\theta$. For this example, the total Burgers vector required is $\mathbf{b}_{\text{SGBD}} = (2a_0/11)[113]$ or two DSC vectors of the $\Sigma=11/(113)/50.48^\circ$ boundary.

The (225) average boundary plane is found by introducing microfacets of a second singular boundary, $\Sigma=3/(111)/109.47^\circ$, into the (113) plane. This faceting must be consistent with the repeat period of the $\Sigma=33/(225)/58.99^\circ$ boundary, while maintaining the low-energy structures of the two boundaries. The required facets can be calculated from the period vector along $(\hat{\mathbf{n}} \times \hat{\mathbf{c}})$, since it gives both the repeat period of the boundary and the boundary plane orientation. For the $\Sigma=33/(225)/58.99^\circ$ boundary the period vector is $(a_0/2)[554]$, while it is $(a_0/2)[332]$ for the $\Sigma=11/(113)/50.48^\circ$ boundary, and $(a_0/2)[112]$ for the $\Sigma=3/(111)/109.47^\circ$ boundary. Since the last two boundaries are centered, there are two SU's in each period. Thus, the period vectors of the SU's, which are $(a_0/4)[332]$ and $(a_0/4)[112]$, are the minimum length microfacets that maintain the low-energy structure of these boundaries. One period of the $\Sigma=33/(225)/58.99^\circ$ GB can be separated into one and a half periods of the $\Sigma=11/(113)/50.48^\circ$ GB and a microfacet of half a period of the $\Sigma=3/(111)/109.47^\circ$ GB:

$$\frac{a_0}{2}[554] = \frac{3a_0}{4}[332] + \frac{a_0}{4}[112]. \quad (6)$$

Figure 7(a) shows this relationship graphically on the $\Sigma=11/(113)/50.48^\circ$ boundary. The grid is the DSC lattice for this boundary.

Unless the period vector for the microfacet is equal to a CSL vector, the RBT vector and thus the structure of the original boundary is not the same on both sides of the microfacet. The SU in Fig. 7(a) above the microfacet is different from the C SU's below the microfacet. The change in the RBT vector introduced by the microfacet can be exactly compensated by inserting two $(a_0/11)[113]$ DSC vectors at the microfacet. This is also the SGBD content required to change from the $\Sigma=11$ misorientation to the $\Sigma=33$ misorientation as calculated above. Figure 7(b) shows how the addition of the SGBD's cancels the change in the RBT vector, so that the structure is the same both above and below the microfacet. For simplicity, the change in the misorientation caused by the SGBD's is not shown.

If the cores of the SGBD's at the microfacets are highly localized, the C SU's above the SGBD's are compressed while those below are expanded normal to the boundary plane. The structure shown in Fig. 7(b) has been relaxed by hand so that the SGBD cores are highly localized. Distortion

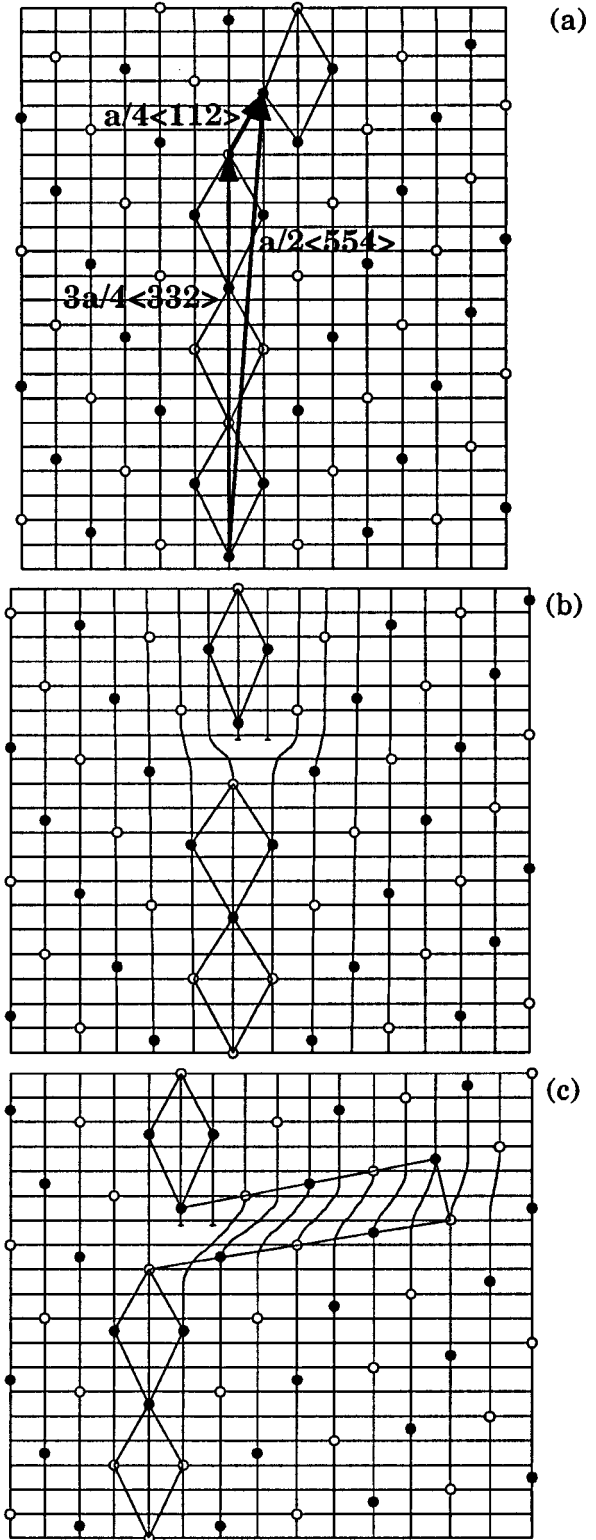


FIG. 7. The three steps in the model of GB dissociation by stacking-fault emission are illustrated for the $\Sigma=33/(225)/58.99^\circ$ vicinal boundary: (a) addition of steps or microfacets, (b) addition of SGBD's, and (c) dissociation of the SGBD's forming stacking faults and a second boundary plane. The structure in (a) is unrelaxed while the structures in (b) and (c) are relaxed by hand. The grid is the DSC lattice of the $\Sigma=11/(113)/50.48^\circ$ singular boundary.

of the **C** SU's is energetically unfavorable. The distortion can be reduced if the SGBD cores dissociate and emit a partial dislocation, leaving the remaining partial at the original boundary plane. The emitted partial dislocation is repelled from the boundary and moves through the perfect crystal to one side creating a planar defect in its wake. A relatively low-energy intrinsic stacking fault is formed if the burgers vector of the partial is $(a_0/6)[112]$. The effect of this dissociation is shown in Fig. 7(c) which was also relaxed by hand. The structure in Fig. 7(c) is identical to the simulated structure in Fig. 4(h) except for the width of the dissociation.

The row of emitted partial dislocations creates a second boundary to the right-hand side of the original. The bending of the $\{111\}$ planes as they cross each boundary can be estimated from Eq. (5) using the Burgers vectors of the two partials. Since the boundaries are no longer symmetric this equation is not strictly valid, but it provides a good approximation. This bending increases the angle of the $\{111\}$ planes closer to the ideal 20° at the **C** SU's and -39° at the **D** SU's, further reducing the distortions of these low-energy SU's. The bending, however, also decreases the $\{111\}$ interplanar spacing in the region between the two boundaries. If the boundary planes are inclined by a few degrees from the original symmetric orientation, the $\{111\}$ planes return to their normal interplanar spacing. This asymmetric orientation has been observed in Cu with both simulations and experiments.⁴⁸ An additional set of SGBD's is required to produce asymmetric tilt GB's. For boundary plane inclinations close to the symmetric orientation, these additional SGBD's do not affect the GB dissociation. These structures were observed in Cu for GB's with inclinations of up to 20° .⁴⁸ In our simulations, the orientation of the boundary plane was fixed by the border conditions so no asymmetric orientations were permitted.

4. Example 2: vicinal $\Sigma=3/(111)/109.47^\circ$ boundary

A second example is the $\Sigma=17/(334)/93.37^\circ$ GB shown in Fig. 4(l) which is vicinal to the $\Sigma=3/(111)/109.47^\circ$ [Fig. 4(m)] singular boundary. For a $\Delta\theta$ of -16.1° , the total Burgers vector of the SGBD's required is $\mathbf{b}_{\text{SGBD}} = -(2a_0/3)[111]$. The (334) average boundary plane is found by introducing (113) microfacets in the (111) plane. The period vector of the $\Sigma=17/(334)/93.37^\circ$ GB $a_0[223]$, is separated into two and one-half periods of the $\Sigma=3/(111)/109.47^\circ$ GB and a microfacet of half a period of the $\Sigma=11/(113)/50.48^\circ$ GB. The reaction is given by

$$a_0[223] = \frac{5a_0}{4}[112] + \frac{a_0}{4}[332]. \quad (7)$$

To minimize the distortions of the **D** SU's, the SGBD's dissociate and two partial dislocations are emitted from the boundary for each **C** SU. The $(a_0/4)[332]$ facets may also be divided into two smaller facets given by the reaction

$$\frac{a_0}{4}[332] = \frac{a_0}{2}[110] + \frac{a_0}{4}[112]. \quad (8)$$

This occurs by the introduction of **A'** SU's that separate the two emitted partial dislocations, along with their stacking faults, as far from each other as possible along the boundary plane.

Either the vicinal $\Sigma=11/(113)/50.48^\circ$ or vicinal $\Sigma=3/(111)/109.47^\circ$ description can be used for any $[1\bar{1}0]$ tilt boundary between these two singular boundaries. It is likely that this mode of GB dissociation occurs in other boundaries as well. Recently,⁴⁹ a wide GB structure was reported for a $\Sigma=3$ asymmetric $\langle 211 \rangle$ tilt boundary in copper. This structure is more complicated than the $\langle 110 \rangle$ tilt boundary structures discussed above and a detailed analysis is needed, but it appears that it was produced by the same type of GB dissociation. In this boundary the emitted partial dislocations are not Shockley partials, and the defects in the newly formed grain are not intrinsic stacking faults. Instead, partial dislocations create planar defects that rearrange the atoms in the new grain such that regions of the bcc structure are formed. Since the energy of the bcc structure is not much higher than the energy of the fcc structure in Cu, it is possible to satisfy the inequality in Eq. (4). Further study is required to determine the singular boundary to which this boundary is vicinal.

B. Structural unit model description of grain-boundary structures

The structural unit model^{12,50} is widely used⁵¹⁻⁵³ to analyze and predict the atomistic structures of GB's. This model describes the structures of boundaries in a given misorientation range, such as the $\langle 110 \rangle$ symmetric tilt boundaries. Although it has never been proven, it is widely believed that the SUM description applies to GB's in all materials. There are several known geometric limitations that restrict the types of boundaries to which the SUM may be applied. These geometric restrictions, which do not include the $\langle 110 \rangle$ symmetric tilt boundaries, are discussed in more detail elsewhere.^{12,54} Many of the GB structures originally used in the development of the SUM were simulated with the DRT pair potential for aluminum²³ which has a high SFE. The results from our simulations are used to investigate the applicability of the SUM to low-SFE GB structures.

1. Structural unit model background

The SUM is used to relate the structures of GB's in a specified misorientation range, i.e., boundaries that have the same rotation axis and average plane orientation. Grain boundaries that have a structure characterized by a repeating sequence of only one type of SU are called favored boundaries. The structures of the GB's between two favored boundaries are predicted to be composed of a combination of the two SU's from the favored boundaries. The ratio and arrangement of the SU's in the nonfavored boundaries are also predicted by the SUM. The ratio of the two different SU's is determined from the period vectors of the SU's and the nonfavored boundary. The SU's are predicted to be arranged in a line on the boundary plane in such a way that the minority SU's are always as far apart as possible. Given the structures of the favored boundaries that delimit a misorientation range, the structure of any nonfavored boundary in this range is predicted by the SUM.

A set of GB structures that follow the predictions of the SUM is shown in Fig. 6. There are three favored boundaries: (1) the $\Sigma = 1/(001)/0^\circ$ perfect crystal orientation [Fig. 4(a)] with the **A** SU; (2) the $\Sigma = 27/(115)/31.59^\circ$ boundary [Fig. 6(c)] with the **B** SU; and (3) the $\Sigma = 11/(113)/50.48^\circ$ boundary [Fig. 6(f)] with the **C** SU. These three boundaries delimit two misorientation ranges: $0^\circ - 31.59^\circ$ and $31.59^\circ - 50.48^\circ$. The structures of the $\Sigma = 33/(118)/20.05^\circ$ [Fig. 6(a)] and $\Sigma = 19/(116)/26.53^\circ$ [Fig. 6(b)] nonfavored boundaries in the first misorientation range are composed of the ratio and arrangement of **A** and **B** SU's predicted by the SUM. The structures of the $\Sigma = 9/(114)/38.94^\circ$ [Fig. 6(d)] and $\Sigma = 57/(227)/44.00^\circ$ [Fig. 6(e)] nonfavored boundaries in the second misorientation range are composed of the predicted ratio and arrangement of **B** and **C** SU's. Several of these same boundaries have been simulated previously with the DRT pair potential for aluminum and were used in the original development of the SUM.¹² The structures shown in Fig. 6 are very similar to the structures found in the earlier simulations even though two different potentials are involved. The only significant difference between the two sets of structures is in the location of the middle atom in the **B** SU.⁵⁵ In the earlier simulations this atom is not centered on the boundary plane, but is located close to a perfect crystal lattice site on one side of the boundary, making the **B** SU asymmetric.

The SUM is closely related to the dislocation model of GB's.^{35,56,57} In the dislocation model, low-angle boundaries are created by networks of primary GB dislocations (GBD's). Large-angle boundaries with misorientations close to singular boundaries are described as having a network of SGBD's superimposed on the structure of the singular boundary. The singular boundaries can be equated with the favored boundaries in the SUM. Neither model can predict *a priori* which boundaries will be favored. In the SUM the nonfavored boundaries are composed of two different SU's. For low-angle boundaries, the majority SU's are the perfect crystal structure and the minority SU's are primary GBD's. In high-angle boundaries the majority SU's contain the dislocation core structure of the nearest favored boundary and the minority SU's are SGBD's of that boundary. The difference between these two models is that the SUM gives the atomic arrangements corresponding to the cores of the GBD's and SGBD's, while the dislocation model makes no predictions about the core structures. Even though the total dislocation content of a GB can always be determined from a geometric dislocation model, the atomistic structure of the dislocation cores cannot always be predicted from the SUM, as is shown in the next section.

2. Application to equilibrium structures

In contrast to the structures in Fig. 6, the same six boundaries simulated with the low-SFE potential in Figs. 4(b)–4(g), do not fit the predictions of the SUM. The $\Sigma = 1/(001)/0^\circ$ [Fig. 4(a)] and $\Sigma = 11/(113)/50.48^\circ$ [Fig. 4(g)] boundaries are favored and the **A** and **C** SU's are found in the boundaries throughout this range, but their ratios and arrangement do not follow the predictions of the SUM. Also, there are other structural elements such as the **B** and **D** SU's and stacking faults emanating from the **C** SU's that are required to fully characterize these boundary structures. Simi-

lar deviations from the predictions of the SUM are apparent in the other $\langle 110 \rangle$ tilt boundaries in Fig. 4. The $\Sigma = 11/(113)/50.48^\circ$ [Fig. 4(g)] and $\Sigma = 3/(111)/109.47^\circ$ [Fig. 4(m)] boundaries are favored and delimit another misorientation range. The **C** and **D** SU's from the favored boundaries are found in the nonfavored boundaries in this range but there are also **A'** SU's and stacking faults. If the $\Sigma = 9/(221)/141.06^\circ$ [Fig. 4(p)] boundary is considered to be favored, even though the **E** SU has two different orientations, then along with the $\Sigma = 3/(111)/109.47^\circ$ boundary a third misorientation range is formed. Other authors have defined favored boundaries using different but closely related SU's to improve the agreement of the SUM with experimentally observed GB structures in SrTiO₃,⁵⁸ although this is not permitted in the original SUM. If one allows for the two **E** SU orientations, the nonfavored boundaries in this range do follow the predictions of the SUM. The $\Sigma = 9/(221)/141.06^\circ$ and $\Sigma = 1/(110)/180^\circ$ [Fig. 4(u)] boundaries delimit a fourth misorientation range. The **E** SU's are found in some of the nonfavored boundaries but only with **A** SU's that do not belong to this range. Similarly, **A'** SU's are found in the $\Sigma = 73/(661)/166.56^\circ$ nonfavored boundary [Fig. 4(t)] but only with **E'** SU's. Finally, the GB structures in Sec. III B 6 that have relaxations along the tilt axis cannot be explained with the SUM.

Although the 0 K equilibrium structures cannot be explained using the SUM, there are selected 0 K metastable structures that do fit the SUM predictions. A set of metastable structures were found for the GB's in range 1 that are identical to the structures in Fig. 6. Most of these structures had very high GB energies and four of the six were not stable at 800 K. For example, in the $\Sigma = 33/(118)/20.05^\circ$ GB, the metastable structure that fits the SUM has a GB energy that is 152 mJ m^{-2} or 17% higher than the equilibrium structure. Thus, the GB structures predicted by the SUM may exist, but they are not necessarily the equilibrium structures or even stable at elevated temperatures.

3. Multiplicity of structures in the structural unit model

As discussed in Sec. III A 2, large number of different structures are found for many boundaries. The SUM has been expanded to include two conditions under which such a multiplicity of structures can be produced.⁵² The first condition applies when one or both of the favored boundaries for a misorientation range have more than one structure. The different favored boundary structures produce more than the normal two SU's for a misorientation range. The nonfavored boundaries can have multiple structures comprised of combinations of the different SU's. Only one structure was found for both the $\Sigma = 1/(001)/0^\circ$ and $\Sigma = 11/(113)/50.48^\circ$ favored boundaries in our simulations and thus, the first condition for a multiplicity of structures is not satisfied. The second condition concerns the RBT vectors of the favored boundaries. If the RBT vectors are different, then their SU's could be incompatible. Two additional SU's that are compatible with the ones from the favored boundaries, but may not themselves be found in any favored boundaries, can appear in the misorientation range. The four SU's create two independent series of boundary structures. The structures of the $\Sigma = 1/(001)/0^\circ$ and $\Sigma = 11/(113)/50.48^\circ$ favored boundaries in range 1 have identical in-plane RBT vectors.

Thus, neither of the two conditions in the SUM provide an explanation for the multiplicity of structures found in range 1. The results are similar for the other tilt-angle ranges.

4. Possible reasons for problems with the structural unit model description

The SUM has been successful in explaining the structures found in at least some $\langle 110 \rangle$ symmetric tilt boundaries. Despite this, we have shown that it does not apply to the GB structures in Fig. 4 for some of the same boundaries. There are three possible reasons for this inconsistency: (1) differences in the computational procedure, (2) differences in the type of potential used, and (3) differences in the properties of the elements being simulated.

Most of the applications of the SUM have been to simulated GB structures, due to the difficulty of observing experimentally the structures of a range of boundaries. The vast majority of these simulations have used some form of energy minimization technique. The effect of different minimization routines is expected to be negligible compared to the effect of different sets of initial configurations. As shown in Sec. III A 2, it is very important when using an energy minimization technique to start with a large number of initial configurations since the accessibility of the 0 K equilibrium structures is often not very large. Earlier simulations generally used a relatively small number of initial configurations, presumably due to the limited computational power available at the time. In our simulations, the 0 K metastable structures that did fit the SUM often had fairly large accessibilities. For example, in the $\Sigma = 27/(115)/31.59^\circ$ GB, the metastable structure that fits the SUM has an accessibility of 45%, versus just 1% for the equilibrium structure [see Fig. 3(a)]. Thus, using a small number of initial configurations may result in finding only the structures that fit the SUM, even though they are not the equilibrium structures. Other procedural differences, including using constant pressure conditions instead of constant volume and differences in the sizes of the computational cells, are not expected to be significant.⁵⁹

All of the early simulations on GB structure were performed with pairwise potentials. These potentials tend to underestimate the importance of coordination effects in metals. As a result, GB structures simulated with pair potentials have large variations in the local density. This is typified by rigid GB structures, where there is little atomic relaxation from the perfect crystal lattice positions and voids are formed in the boundaries. In EAM potentials, on the other hand, the dominant term is the embedding energy which is a function of the electron density. Structures simulated with EAM potentials tend to have more extensive atomic relaxations and smaller voids in the boundaries. An example of this difference is found in the **B** SU of the $\Sigma = 27/(115)/31.59^\circ$ boundary [Fig. 6(c)] in aluminum. When simulated with an EAM potential the middle atom is located at the center of this SU which minimizes local density fluctuations. In the same SU simulated with the DRT pair potential this atom is located on one side, nearly at a perfect crystal lattice position, breaking the mirror symmetry of the GB structure.¹² While making the local density on one side nearly ideal, this creates a large void in the GB. Simulations using pair potentials, with their more rigid boundary structures, tend to have a better agree-

ment with the SUM. There are, however, a few examples of structures that fit the SUM that have been simulated with EAM-type potentials.⁵³

Probably the most important difference is in the properties of the elements that are being simulated. Both the earlier simulations and the structures in Fig. 6 are for aluminum, whereas the structures in Fig. 4 are for a low-SFE fcc metal. The low SFE favors a greater delocalization of the GBD's resulting in the wider structures that are found. Other material properties such as the elastic constants may also play an important role in determining the structures of some boundaries. Some of the effects of delocalization of the GBD's on the SUM have been pointed out previously.^{35,60} If the delocalization is not too severe it simply results in distortions of the SU's. To reduce the distortions, nonfavored boundaries, which are called multiple unit reference structures (MURS),⁵⁶ can be used as additional delimiting boundaries to make the misorientation ranges smaller. The predictive value of the SUM is reduced by the use of MURS because a larger number of delimiting boundaries are required for the same misorientation range, but the distortion of the SU's is reduced. The structures in Fig. 4 demonstrate that in some materials, delocalization can become large enough that different modes of GB relaxation produce structures with lower GB energies than are possible with a SUM-type structure. These relaxation modes can include faceting, introduction of GB steps, changes in the RBT vector and GB dissociation. The SUM cannot predict for what boundaries these different modes of GB relaxation will occur or describe the structures when they do.

Despite the problems illustrated above, the SUM has been found to be useful for describing GB structures in many materials. Even when the detailed predictions of the SUM do not hold, such as for the structures in Fig. 4, there are still SU's in the boundaries. Some of these characteristic low-energy arrangements of atoms are found in many different boundaries, often beyond the range allowed in the SUM. There may not even be a favored boundary for some frequently occurring SU's. The GB structures formed by these SU's are more like the structures in the original polyhedral unit model⁶¹ than the SUM.

V. CONCLUSIONS

Twenty-one $\langle 110 \rangle$ symmetric tilt GB's are investigated with atomistic simulations using an embedded-atom method (EAM) potential for a low stacking-fault energy (SFE) fcc metal. The computational procedure involves the use of a large number of initial configurations with different rigid-body translation vectors. This procedure allows for both the 0 K equilibrium and metastable structures to be found with lattice statics simulations. The stability of these structures at an elevated temperature is also investigated by MC annealing. The following conclusions are reached from these simulations.

(1) The 0 K equilibrium structures are often difficult to find with an energy minimization technique. The accessibility of the equilibrium structures, which is the percentage of the initial configurations that relax to those structure, is less than 15% for over half of the boundaries investigated. Many of these equilibrium structures would not have been found if

a smaller number of initial configurations had been used.

(2) Most tilt boundaries have a large multiplicity of structures. Seventeen of the 21 boundaries have four or more structures at 0 K. The number of structures appears to be related to the size of the cell of non-identical displacements for each boundary.

(3) Many 0 K metastable structures remain stable at elevated temperatures. At a temperature of 800 K, over half of the boundaries investigated have three or more stable structures. The energy barriers separating different GB structures are often too high to be overcome by thermal fluctuations. Thus, in elevated temperature simulations, as well as in real materials, a multiplicity of structures may exist that cannot be ignored.

(4) Grain-boundary structures in low-SFE materials may be quite wide due to delocalization or dissociation of the primary or secondary GB dislocations. These structures tend to have stronger local atomic relaxations than are found in GB's in higher-SFE materials. The atomic relaxations also tend to make the local density more uniform, such that voids are not found in the boundaries.

(5) Some 0 K equilibrium structures are found that have local atomic relaxations along the tilt axis that disrupt the continuity of the planes perpendicular to this direction. Although it had been previously argued that such structures should not be stable, many did remain stable during MC annealing at 800 K.

The 0 K equilibrium structures are used in discussions of two main topics: GB dissociation by the emission of stacking-faults and the usefulness of the structural unit model (SUM) in describing GB structures in low-SFE fcc metals. Several conclusions are reached from these discussions.

(1) The simulated GB's with tilt angles between 50.48° and 109.47° have dissociated by emitting stacking faults. Similar GB structures have been observed experimentally in several boundaries in three low-SFE fcc metals.

(2) This form of GB dissociation may occur in GB's that are vicinal to singular boundaries. The secondary GB dislocations in the vicinal boundary dissociate by emitting Shockley partial dislocations. The partial dislocations move to one

side of the original boundary plane, thereby creating stacking faults and a second boundary plane.

(3) This type of GB dissociation is unlike previously recognized types, since the newly formed grain is not free of residual defects from the dissociation process. The two boundaries are not free to move apart indefinitely because of the excess free energy per unit volume associated with these defects.

(4) The SUM is not found to be useful for describing the GB structures found in low-SFE fcc metals. The extensive local atomic relaxations and delocalized or dissociated GB dislocations result in 0 K equilibrium structures that are produced by modes of GB relaxation that are incompatible with the SUM description.

(5) The GB structures that are predicted from the SUM are found in some of the boundaries, but these structures typically have high GB energies. The other 0 K metastable structures that are found, cannot be predicted using the conditions in the SUM for a multiplicity of structures.

(6) The SUM has been widely used to describe and predict GB structures in many materials. Even when the predicted structures are not found, there are still SU's in the boundaries. The GB structures formed by these SU's, however, are more like the structures in the original polyhedral unit model than the SUM.

ACKNOWLEDGMENTS

J.D.R. acknowledges the support of a Computational Sciences Graduate Fellowship program at Ames Laboratory, Ames, Iowa, the McCormick School of Engineering and Applied Sciences for financial support, the Alexander von Humboldt Foundation for partial support through the Max Planck Research Prize of DNS, and the National Energy Research Supercomputer Center for computer time. D.N.S. acknowledges support by the National Science Foundation (Grant No. DMR-9319074, Dr. B. MacDonald, grant officer). This work made use of the MRL Central Facilities at Northwestern University, which are supported by the National Science Foundation under award No. DMR-9120521. Dr. D. Udler is thanked for helpful discussions.

¹D. N. Seidman, B. W. Krakauer, and D. Udler, *J. Phys. Chem. Solids* **55**, 1035 (1994); R. W. Balluffi, in *Interfacial Segregation*, edited by W. C. Johnson and J. M. Blakely (American Society for Materials, Metals Park, OH, 1979), p. 193.

²N. L. Peterson, in *Grain Boundary Structure and Kinetics* (American Society for Metals, Metals Park, OH, 1980), p. 209; G. Martin and G. Perrailon, *ibid.*, p. 239.

³D. A. Smith, in *Materials Interfaces*, edited by D. Wolf and S. Yip (Chapman & Hall, New York, 1992), p. 212; D. A. Smith, C. M. F. Rae, and C. R. M. Grovenor, in *Grain Boundary Structure and Kinetics* (Ref. 2), p. 337; M. F. Ashby, *Surf. Sci.* **31**, 498 (1972).

⁴R. Monzen *et al.*, *J. Phys. (Paris) Colloq.* **51**, C1-269 (1990).

⁵G. Palumbo and K. T. Aust, in *Materials Interfaces* (Ref. 3), p. 190; *Acta Metall. Mater.* **38**, 2343 (1990).

⁶K. T. Aust, U. Erb, and G. Palumbo, *Mater. Sci. Eng. A* **176**, 329 (1994); J. S. Wang and P. M. Anderson, *Acta Metall. Mater.* **39**, 779 (1991).

⁷J. W. Cahn, *J. Phys. (Paris) Colloq.* **43**, C6-199 (1982).

⁸D. Wolf, *J. Phys. (Paris) Colloq.* **46**, C4-197 (1985).

⁹A. P. Sutton and R. W. Balluffi, *Acta Metall.* **35**, 2177 (1987).

¹⁰D. Hofmann and F. Ernst, *Interface Sci.* **2**, 201 (1994).

¹¹K. L. Merkle, *J. Phys. Chem. Solids* **55**, 991 (1994).

¹²A. P. Sutton and V. Vitek, *Philos. Trans. R. Soc. London Ser. A* **309**, 1 (1983).

¹³The term "border conditions" is used in place of the more conventional "boundary conditions" to eliminate confusion with the actual grain boundaries in the computational cells.

¹⁴D. Udler and D. N. Seidman, *Phys. Status Solidi B* **172**, 267 (1992).

¹⁵M. S. Daw and M. I. Baskes, *Phys. Rev. Lett.* **50**, 1285 (1983); M. S. Daw and M. I. Baskes, *Phys. Rev. B* **29**, 6443 (1984).

¹⁶M. S. Daw, *Phys. Rev. B* **39**, 7441 (1989).

¹⁷M. S. Daw, S. M. Foiles, and M. I. Baskes, *Mater. Sci. Rep.* **9**, 251 (1993).

- ¹⁸M. S. Daw (private communication).
- ¹⁹S. M. Foiles, M. I. Baskes, and M. S. Daw, *Phys. Rev. B* **33**, 7983 (1986).
- ²⁰L. E. Murr, *Interfacial Phenomena in Metals and Alloys* (Addison-Wesley, Reading, MA, 1975), p. 145.
- ²¹A. Howie and P. R. Swann, *Philos. Mag.* **6**, 1215 (1961).
- ²²F. Ercolessi and J. B. Adams, *Europhys. Lett.* **26**, 583 (1994).
- ²³L. Dagens, M. Rasolt, and R. Taylor, *Phys. Rev. B* **11**, 2726 (1975).
- ²⁴V. Vitek, *Scr. Metall.* **9**, 611 (1975).
- ²⁵S. M. Foiles, M. I. Baskes, and M. S. Daw, *Interfacial Structure, Properties, and Design*, edited by M. H. Yoo, W. A. T. Clark, and C. L. Briant, MRS Symposia Proceedings No. 122 (Materials Research Society, Pittsburgh, 1988).
- ²⁶R. C. Pond, *Proc. R. Soc. London Ser. A* **357**, 463 (1977).
- ²⁷V. Vitek, A. P. Sutton, D. A. Smith, and R. C. Pond, in *Grain Boundary Structure and Kinetics* (Ref. 2), p. 115.
- ²⁸H. Grimmer, W. Bollman, and D. H. Warrington, *Acta Crystallogr. Sect. A* **30**, 197 (1974).
- ²⁹R. Fletcher and C. M. Reeves, *Comput. J.* **7**, 149 (1964).
- ³⁰Systematic displacements of the atoms in the bicrystal due to thermal expansion and small random displacements from statistical noise must first be subtracted to identify structural changes.
- ³¹D. Wolf, *Acta Metall. Mater.* **38**, 781 (1990).
- ³²G. C. Hasson and C. Goux, *Scr. Metall.* **5**, 889 (1971); A. Otsuki and M. Mizuno, *Trans. Jpn. Inst. Met. Suppl.* **27**, 789 (1986).
- ³³A. P. Sutton and R. W. Balluffi, *Interfaces in Crystalline Materials* (Clarendon Press, Oxford, 1995), p. 132.
- ³⁴J. D. Bernal, *Nature* **185**, 68 (1960).
- ³⁵R. W. Balluffi and P. D. Bristowe, *Surf. Sci.* **144**, 28 (1984).
- ³⁶W. T. Read, *Dislocations in Crystals* (McGraw-Hill, New York, 1953), p. 96.
- ³⁷R. C. Pond, D. A. Smith, and V. Vitek, *Acta Metall.* **27**, 235 (1979).
- ³⁸For example, the HREM used in Ref. 49 has a point-to-point resolution of 0.12 nm, which is just sufficient to image the atomic columns along the ⟨211⟩ axis in copper.
- ³⁹C. T. Forwood and L. M. Clarebrough, *Acta Metall.* **32**, 757 (1984); see also Ref. 33, p. 402.
- ⁴⁰J. D. Rittner, D. N. Seidman, and K. L. Merkle, *Phys. Rev. B* **53**, R4241 (1996).
- ⁴¹A. G. Crocker and B. A. Faridi, *Acta Metall.* **28**, 549 (1980).
- ⁴²H. Ichinose and Y. Ishida, *J. Phys. (Paris) Colloq.* **46**, C4-39 (1985); H. Ichinose, Y. Ishida, N. Baba, and K. Kanaya, *Philos. Mag. A* **52**, 51 (1985).
- ⁴³K. L. Merkle, *J. Phys. (Paris) Colloq.* **51**, C1-251 (1990); *Ultramicroscopy* **37**, 130 (1991).
- ⁴⁴F. Ernst *et al.*, *Phys. Rev. Lett.* **69**, 620 (1992).
- ⁴⁵D. Hofmann and F. Ernst, *Ultramicroscopy* **53**, 205 (1994).
- ⁴⁶For definitions of singular, vicinal and general boundaries see Ref. 33, p. xxix.
- ⁴⁷W. T. Read and W. Shockley, *Phys. Rev.* **78**, 275 (1950); F. C. Frank, in *Symposium on the Plastic Deformation of Crystalline Solids* (Carnegie Institute of Technology, Pittsburgh, PA, 1950), p. 150.
- ⁴⁸U. Wolf, F. Ernst, T. Muschik, M. W. Finnis, and H. F. Fischmeister, *Philos. Mag. A* **66**, 991 (1992).
- ⁴⁹C. Schmidt, F. Ernst, M. W. Finnis, and V. Vitek, *Phys. Rev. Lett.* **75**, 2160 (1995).
- ⁵⁰G. H. Bishop and G. Chalmers, *Scr. Metall.* **2**, 133 (1968).
- ⁵¹D. A. Smith, *J. Phys. (Paris) Colloq.* **49**, C5-63 (1988); W. Krakow, *Philos. Mag. A* **63**, 233 (1991); M. J. Mills, *Mater. Sci. Eng. A* **166**, 35 (1993); J.-M. Penisson, *J. Phys. (Paris) Colloq.* **49**, C5-87 (1988); J.-M. Penisson, T. Nowicki, and M. Biscondi, *Philos. Mag. A* **58**, 947 (1988); A. Bourret, *J. Phys. (Paris) Colloq.* **46**, C4-27 (1985); M. D. Vaudin, B. Cunningham, and D. G. Ast, *Scr. Metall.* **17**, 191 (1983); N. D. Browning *et al.*, *Interface Sci.* **2**, 397 (1995); A. P. Sutton and V. Vitek, *Philos. Trans. R. Soc. London Ser. A* **309**, 37 (1983); D. Schwartz, V. Vitek, and A. P. Sutton, *Philos. Mag. A* **51**, 499 (1985); J. Thibault *et al.*, *Mater. Sci. Eng. A* **164**, 93 (1993).
- ⁵²G. J. Wang, A. P. Sutton, and V. Vitek, *Acta Metall.* **32**, 1093 (1984).
- ⁵³G. J. Ackland, G. Tichy, V. Vitek, and M. W. Finnis, *Philos. Mag. A* **56**, 735 (1987).
- ⁵⁴A. P. Sutton and R. W. Balluffi, *Philos. Mag. Lett.* **61**, 91 (1990); A. P. Sutton, *ibid.* **59**, 53 (1989).
- ⁵⁵The SU's in Ref. 12 are defined differently and are labeled **C**, **A**, **B** instead of **A**, **B**, **C** for the $\Sigma=1/(001)/0^\circ$, $\Sigma=27/(115)/31.59^\circ$, and $\Sigma=11/(113)/50.48^\circ$ boundaries, respectively.
- ⁵⁶A. P. Sutton, R. W. Balluffi, and V. Vitek, *Scr. Metall.* **15**, 989 (1981).
- ⁵⁷P. D. Bristowe and R. W. Balluffi, *J. Phys. (Paris) Colloq.* **46**, C4-155 (1985).
- ⁵⁸N. D. Browning *et al.*, *Interface Sci.* **2**, 397 (1995).
- ⁵⁹As a test, several boundaries were simulated with constant volume conditions and different cell sizes. The same GB structures were found in all cases.
- ⁶⁰A. P. Sutton, *Philos. Mag. Lett.* **59**, 53 (1989).
- ⁶¹R. C. Pond, D. A. Smith, and V. Vitek, *Scr. Metall.* **12**, 699 (1978).